Journal of Power Sources 195 (2010) 3882–3886

Contents lists available at ScienceDirect

Journal of Power Sources

journal homepage: www.elsevier.com/locate/jpowsour

Short Communication

Direct operation of cone-shaped anode-supported segmented-in-series solid oxide fuel cell stack with methane

Yaohui Bai [a,b,c], Chuanling Wang [a,b,c], Jiao Ding [a,b,c], Chao Jin [a,b,c], Jiang Liu [a,b,c,*]

[a] School of Chemistry and Chemical Engineering, South China University of Technology, Guangzhou 510641, PR China
[b] The Key Laboratory of Enhanced Heat Transfer and Energy Conversation, Ministry of Education, Guangzhou 510641, PR China
[c] The Key Laboratory of New Energy Technology for Guangdong Universities, Department of Education of Guangdong Province, Guangzhou 510641, PR China

ARTICLE INFO

Article history:
Received 20 November 2009
Received in revised form
19 December 2009
Accepted 22 December 2009
Available online 13 January 2010

Keywords:
Solid oxide fuel cell
Cone-shaped
Segmented-in-series
Stack
Methane

ABSTRACT

Operation of cone-shaped anode-supported segmented-in-series solid oxide fuel cell (SIS-SOFC) stack directly on methane is studied. A cone-shaped solid oxide fuel cell stack is assembled by connecting 11 cone-shaped anode-supported single cells in series. The 11-cell-stack provides a maximum power output of about 8 W (421.4 mW cm^{-2} calculated using active cathode area) at 800 °C and 6 W (310.8 mW cm^{-2}) at 700 °C, when operated with humidified methane fuel. The maximum volumetric power density of the stack is 0.9 W cm^{-3} at 800 °C. Good stability is observed during 10 periods of thermal cycling test. SEM-EDX measurements are taken for analyzing the microstructures and the coking degrees.

1. Introduction

Segmented-in-series solid oxide fuel cells (SIS-SOFCs) have been attracting more and more attentions [1–4]. The advantages of SIS-SOFCs over tubular SOFCs include simplification of the external connecting, decrease of the current path and increase of the volumetric energy density. Being light and compact, it is very promising for portable application.

There are two main configurations of SIS-SOFCs: banded tubular SIS-SOFCs and cone-shaped anode-supported SIS-SOFCs. Banded tubular SIS-SOFCs, comprising porous insulating substrate and anode/electrolyte/cathode tri-layers, have excellent redox stability and extended range of coke-free operation conditions due to the thinness of anode membrane and the porous substrate barrier layer [5–7]. Fig. 1 shows the schematic illustration of banded tubular SIS-SOFCs. However, banded tubular SIS-SOFCs, with the width of each single cell unit more than 10 mm, have low power density due to large sheet resistance from the relatively thin electrodes. Barnett's research group prepared banded tubular SIS-SOFCs on partially stabilized zirconia (PSZ) flattened-tube supports. They got a satisfying maximum power density of 0.9 W cm^{-2} at 800 °C by decreasing the width of each cell unit to 1.4 mm and increasing the cathode thickness to 91 μm [8]. However, the decrease of the cell width complexes the fabricating process and restricts the total output power. Moreover, the insulating substrate may increase the concentration polarization at high current density.

Cone-shaped anode-supported SIS-SOFCs stack is a novel design proposed by Liu [9]. Fig. 2 shows the schematic diagram. As can be seen, the SIS-SOFCs stack is composed of several cone-shaped single SOFCs connected in electrical and gas flowing series. The cell with one end closed is noted as Cell 1. The cell next to Cell 1 is Cell 2, then Cell 3, etc. Compared with the banded tubular SIS-SOFCs, cone-shaped SIS-SOFCs prepared on the anode substrates decrease the concentration polarization at high current density by eliminating the insulating substrate. Moreover, cone-shaped anode-supported SIS-SOFCs stack has smaller sheet resistance and the fabricating process is simpler. Ding and Liu [10] have fabricated a two-cell-stack based on the cone-shaped anode-supported SOFC and demonstrated its feasibility with hydrogen as fuel.

Direct-methane SOFCs are of interest because natural gas is a widely available fuel and has higher energy density than that of hydrogen [11–15]. Single SOFC operated with methane has been well investigated. However, to our best knowledge, there is a lack of investigation on cone-shaped anode-supported SOFC stack operated with methane. In this paper, we investigated the performance of an 11-cell-stack operated on methane. Its electrochemical performance, thermal cycling stability, microstructure, and coking are presented and analyzed in detail.

* Corresponding author. Tel.: +86 020 22236168; fax: +86 020 22236168.
E-mail address: jiangliu@scut.edu.cn (J. Liu).

0378-7753/$ – see front matter © 2010 Elsevier B.V. All rights reserved.
doi:10.1016/j.jpowsour.2009.12.110

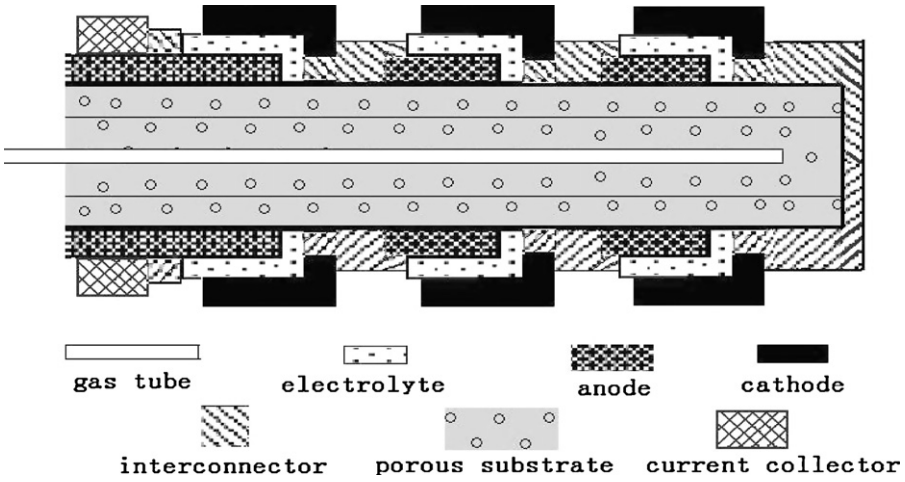

Fig. 1. The schematic of the banded tubular SIS-SOFCs stack.

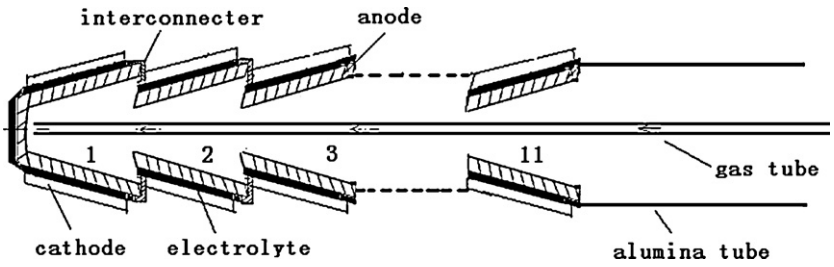

Fig. 2. The schematic of the cone-shaped anode-supported SIS-SOFCs stack.

2. Experimental

2.1. SIS-SOFC stack preparation

The cone-shaped anode-supported SIS-SOFC stack fabricating method comprises three major processes: dip coating, brush painting, and stack assembling. The anode substrate was fabricated by dip coating technique with well-mixed NiO powder (INCO Canada) and 8 mol% YSZ powder (Tosoh, Japan). After sintered at 1200 °C for 2 h, the anode substrate was dipped in YSZ slurry and co-fired at 1400 °C for 4 h. Next, the cathode of LSM/YSZ and LSM was brush painted on the electrolyte. Then 11 cone-shaped anode-supported SOFCs were assembled in electrical and gas flow series according to the configuration of Fig. 2. The detailed fabrication process was described in our previous report [16]. Fig. 3 shows the photo of the cone-shaped anode-supported SOFCs. Fig. 4 shows the photo of the 11-cell-stack. The total length of the stack is 9.5 cm and the diameter of the cone-shaped SOFC is 1.1 cm. The total effective cathode area of the 11-cell-stack is 18.7 cm^2.

2.2. SIS-SOFCs stack testing

The 11-cell-stack was reduced at 600 °C for 1 h when 3 vol.% water humidified hydrogen (150 ml min^{-1}) was supplied at the anode side. Then the hydrogen was switched to humidified methane (100 ml min^{-1}). The 11-cell-stack was tested in the

Fig. 3. The photo of the cone-shaped anode-supported SOFCs.

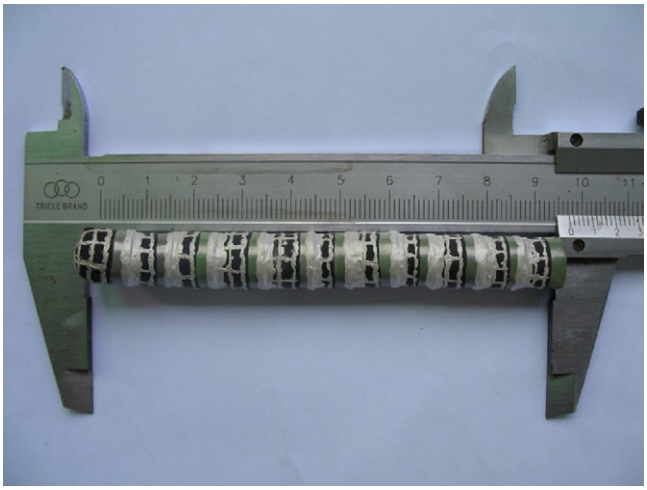

Fig. 4. The photo of the 11-cell-stack.

temperature range of 600–800 °C, with the cathode side exposed to ambient air. After that, thermal cycling tests were performed using moist hydrogen (150 ml min^{-1}) as fuel. Each period of thermal cycling test was carried out by raising the temperature from 300 to 800 °C, measuring the OCV of the stack, and then lowering the temperature to 300 °C.

The electrochemical performance of the stack was tested by a four-probe method using IviumStat electrochemical analyzer (Ivium Technologies B.V., Netherlands). After these tests, the microstructures of the cells were characterized by a scanning electron microscope (SEM, Philips XL-30FEG, Holland). SEM-EDX measurements were taken at the anode surfaces of Cell 1, Cell 3 and Cell 5.

3. Results and discussion

3.1. Electrochemical performance of the 11-cell-stack

Fig. 5 shows the *I–V–P* characteristics comparison of the stack operated at 600 °C using moist hydrogen (150 ml min^{-1}) and methane (100 ml min^{-1}) as fuel. As can be seen, the open circuit voltage (OCV) of the 11-cell-stack is about 10.5 V. The stack provides a maximum power density as high as 84.1 and 55.1 mW cm^{-2} at 600 °C using moist hydrogen and methane as fuel, respectively.

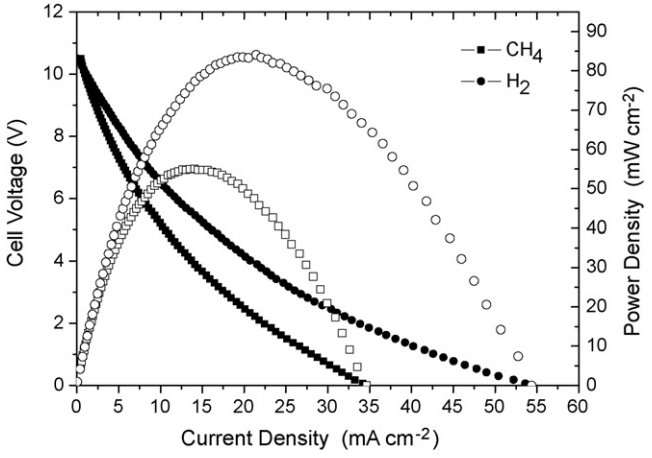

Fig. 5. The *I–V–P* characteristics comparison of the stack operated at 600 °C using moist hydrogen (150 ml min^{-1}) and methane (100 ml min^{-1}) as fuel and ambient air as oxidant.

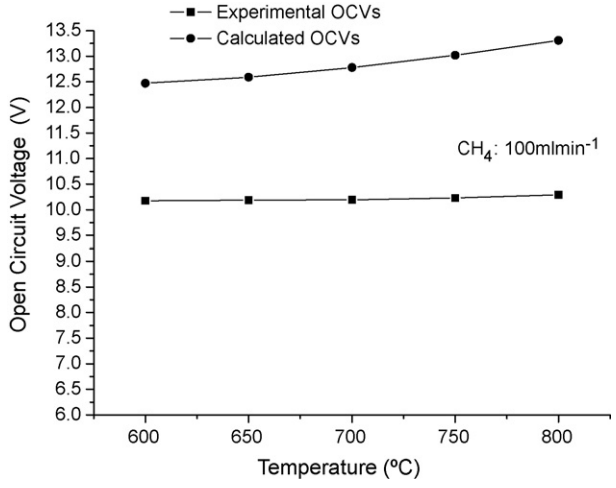

Fig. 6. The open circuit voltage of the 11-cell-stack at different operating temperatures.

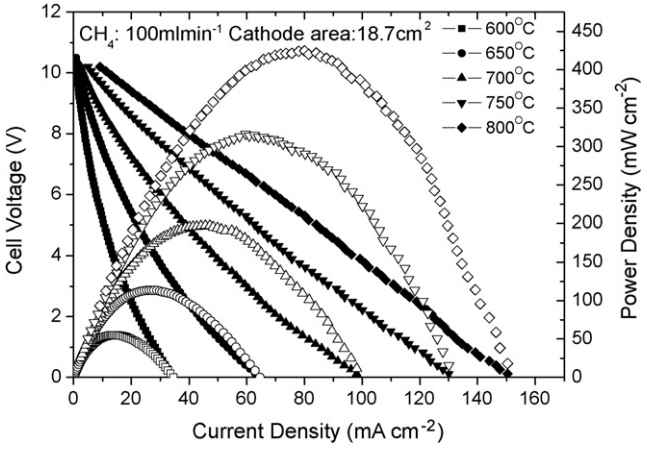

Fig. 7. The *I–V–P* characteristics of the 11-cell-stack at different operating temperatures.

The maximum power density of the stack using moist hydrogen as fuel is about 34.4%, higher than that using methane. The result 34.4% is higher than the 20% in the previous reports [13] due to the flow rate of the hydrogen gas was higher than that of the methane gas.

Fig. 6 shows the OCVs of the stack using methane (100 ml min^{-1}) as fuel at different temperatures. As can be seen, the OCV increases with temperature, of which result accords with the calculation from Nernst equation. In the testing temperature range, the OCVs of the 11-cell-stack are higher than 10.1 V and the average OCV of each cell is about 0.93 V, which is close to the theoretical OCV value. It demonstrates that the electrolyte layer is dense and the sealing technique is acceptable for the stack assembling. Fig. 7 is the *I–V–P* characteristics of the 11-cell-stack using methane

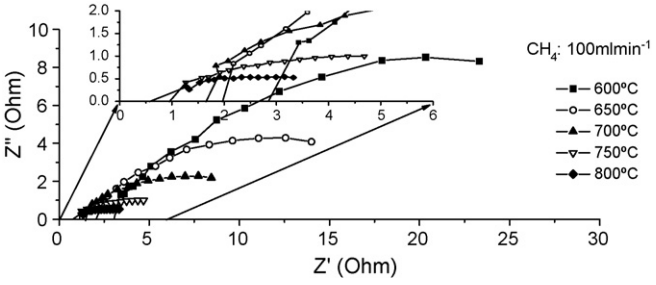

Fig. 8. The electrochemical impedance spectra of the 11-cell-stack measured from 600 to 800 °C.

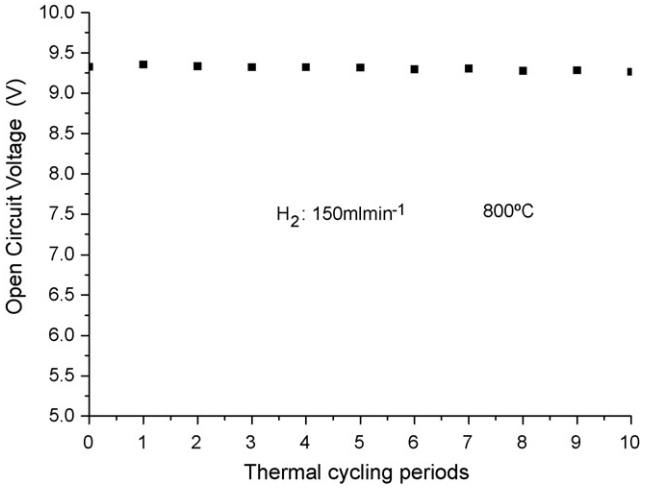

Fig. 9. The OCVs of the 11-cell-stack at 800 °C for each period of thermal cycling.

($100\,ml\,min^{-1}$) as fuel at different testing temperatures. We can see that the stack provides a maximum power output of about 8 W ($421.4\,mW\,cm^{-2}$ calculated using active cathode area) at 800 °C and 6 W ($310.8\,mW\,cm^{-2}$) at 700 °C. The volumetric of the stack is about $0.9\,W\,cm^{-3}$ at 800 °C. At lower temperature, the voltage versus current is concave up, indicating that activation polarization dominates the total resistance. At higher temperature, the curve of voltage versus current becomes more linear, indicating that the activation polarization decreases evidently and the ohmic resistance becomes more influential. The electrochemical impedance spectra of the 11-cell-stack measured at different temperatures are shown in Fig. 8. For the whole cell impedance, the intercepts of the real axis at high-frequency correspond to the cell ohmic resistance while the arcs at low-frequency are the overall electrodes polarization resistance including those from both anode and cathode. It is obvious that at lower temperatures the polarization resistance is much larger than the ohmic resistance. Therefore, further improvement of electrode activity and electrode/electrolyte interface for cone-shaped anode-supported SIS-SOFCs stack is required to get higher performance at lower temperatures.

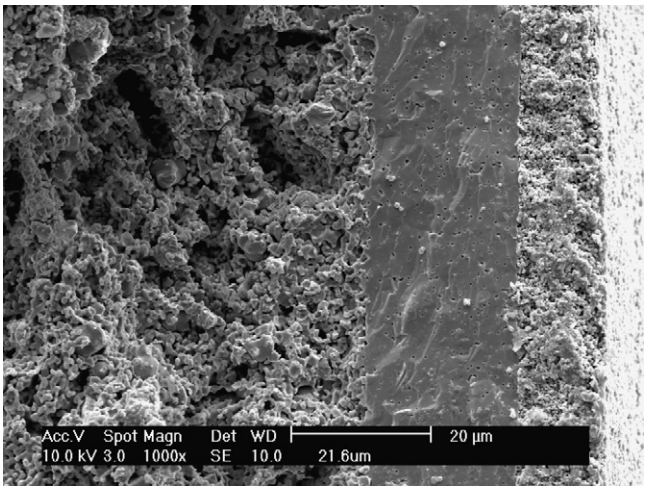

Fig. 10. SEM micrograph of cross-section of SOFC after testing.

3.2. Thermal cycling stability of the 11-cell-stack

Fig. 9 shows the stability of the 11-cell-stack through 10 periods thermal cycling testing using moist hydrogen ($150\,ml\,min^{-1}$) as fuel and ambient air as oxidant. The stack OCV maintains at about 9.3 V at 800 °C after 10 periods of thermal cycling tests, indicating that good stability can be attained with the cone-shaped anode-supported SIS-SOFCs design and that the decay of the sealing effect is negligible. Similar work on a two-cell-stack has been done by

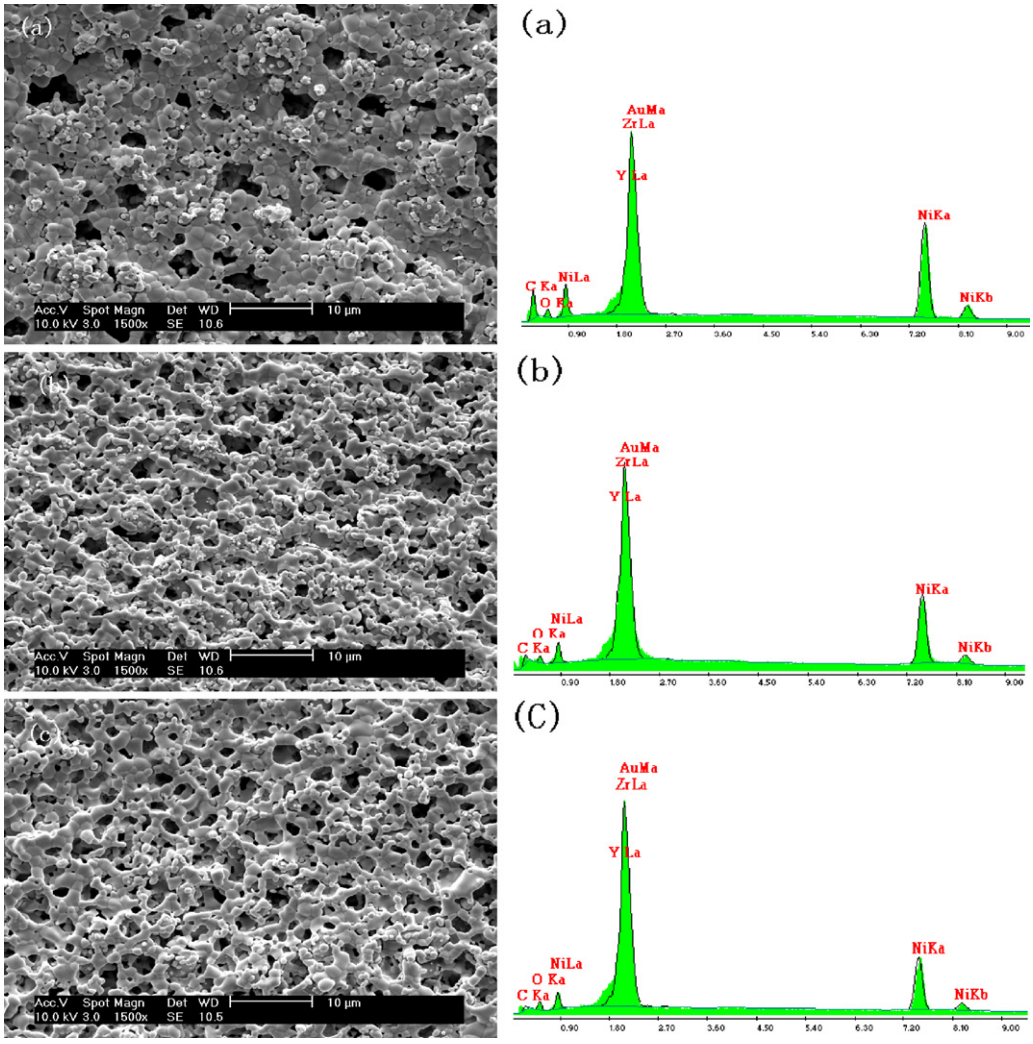

Fig. 11. SEM micrographs and EDX spectra taken from anode surfaces after testing (a) Cell 1, (b) Cell 3 (c) Cell 5.

some of our coauthors [10]. The stability of the 11-cell-stack shows that the fabricating technique for the two-cell-stack also works well for multi-cell-stack. The capability of enduring thermo-mechanical stresses through the thermal cycling test is significant for portable application.

The thermal cycling stability of a multi-cell-stack in methane, along with the operation life, should be significantly influenced by the operating current, and that investigation involves a lot of work. The corresponding research is in our next plan.

3.3. Microstructures of the as-prepared samples

Fig. 10 is a representative facture cross-sectional SEM image of the cell, showing a 20 μm-thick YSZ film. As can be seen, the electrode layers are porous while the YSZ electrolyte film is quite dense. All the layers are reasonably flat and uniform, with intimate contact at the interfaces.

Fig. 11 shows SEM-EDX spectra taken from the anode surface of Cell 1, Cell 3 and Cell 5, respectively, after the stack had been tested in methane. Fig. 11(a) shows a clear evidence of carbon deposition: the EDX spectrum shows a strong carbon peak and the image shows stopped holes by carbon. Fig. 10(b) shows slighter carbon on the anode surface and Fig. 10(c) shows the lowest carbon peak. That is because the products of the cell reaction, CO_2 and H_2O, increase along the path from the first cell (Cell 1) to the last one in the stack. CO_2 and H_2O on the anode side can increase the partial oxygen pressure which is propitious to restrain coking.

4. Conclusion

An 11-cell-stack of the cone-shaped anode-supported segmented-in-series SOFC design has been successfully developed. The maximum power output of 8 W at 800 °C and 6 W at 700 °C, and the volumetric power density of 0.9 W cm^{-3} at 800 °C have demonstrated the feasibility of the design and the corresponding techniques for fabricating the stack. 10 periods of thermal cycling test shows that the cone-shaped anode-supported SIS-SOFC stack has good thermo-mechanical properties and that the cone-shaped anode-supported SIS-SOFCs stack is highly promising for portable applications.

Moreover, the SEM-EDX spectra show that the coking degrees are different with the different positions in the stack. So we plan to append different kinds and amounts of catalyst on the cells according to different positions in the stack to restrict the coking in future study.

Acknowledgements

Financial supports from the National “863” program of China (grant no. 2007AA05Z136), the Department of Science and Technology of Guangdong Province (grant no. 2005B50101007) and Department of Education of Guangdong Province (grant no. B15-N9060210) are gratefully acknowledged.

References

[1] F.J. Gardner, M.J. Day, N.P. Brandon, M.N. Pashley, M. Cassidy, J. Power Sources 86 (2000) 122–129.
[2] N.Q. Minh, J. Am. Ceram. Soc. 76 (1993) 563–588.
[3] T.S. Lai, S.A. Barnett, J. Power Sources 147 (2005) 85–94.
[4] D. Cui, M. Cheng, J. Power Sources 195 (2010) 1435–1440.
[5] K. Fujita, T. Somekawa, K. Horiuchi, Y. Matsuzaki, J. Power Sources 193 (2009) 130–135.
[6] H. Zhu, A.M. Colclasure, R.J. Kee, Y. Lin, S.A. Barnett, J. Power Sources 161 (2006) 413–419.
[7] M.R. Pillai, D. Gostovic, I. Kim, S.A. Barnett, J. Power Sources 163 (2007) 960–965.
[8] T.S. Lai, S.A. Barnett, J. Power Sources 164 (2007) 742–745.
[9] J. Liu, Chinese Patent: CN100347897.
[10] J. Ding, J. Liu, J. Power Sources 193 (2009) 769–773.
[11] J. Liu, S.A. Barnett, Solid State Ionics 158 (2003) 11–16.
[12] Z.L. Zhan, Y.B. Lin, M. Pillai, I. Kim, S.A. Barnett, J. Power Sources 161 (2006) 460–465.
[13] Y.B. Lin, Z.L. Zhan, J. Liu, S.A. Barnett, Solid State Ionics 176 (2005) 1827–1835.
[14] Y.B. Lin, Z.L. Zhan, S.A. Barnett, J. Power Sources 158 (2006) 1313–1316.
[15] S. McIntosh, R.J. Gorte, Chem. Rev. 104 (2004) 4845–4865.
[16] Y.H. Bai, J. Liu, C.L. Wang, Int. J. Hydrogen Energy 34 (2009) 7311–7315.